Chin. Ann. Math.
30B(5), 2009, 483–504
DOI: 10.1007/s11401-009-0200-8

Chinese Annals of Mathematics, Series B

Nonlinearly Coupled KdV Equations Describing the Interaction of Equatorial and Midlatitude Rossby Waves**

Joseph A. BIELLO*

(*Dedicated to Professor Andrew Majda on the Occasion of his* 60*th Birthday*)

Abstract Amplitude equations governing the nonlinear resonant interaction of equatorial baroclinic and barotropic Rossby waves were derived by Majda and Biello and used as a model for long range interactions (teleconnections) between the tropical and midlatitude troposphere. An overview of that derivation is presented and geared to readers versed in nonlinear wave theory, but not in atmospheric sciences. In the course of the derivation, two other sets of asymptotic equations are presented: the long equatorial wave equations and the weakly nonlinear, long equatorial wave equations. A linear transformation recasts the amplitude equations as nonlinear and linearly coupled KdV equations governing the amplitude of two types of modes, each of which consists of a coupled tropical/midlatitude flow. In the limit of Rossby waves with equal dispersion, the transformed amplitude equations become two KdV equations coupled only through nonlinear fluxes. Four numerical integrations are presented which show (i) the interaction of two solitons, one from either mode, (ii) and (iii) the interaction of a soliton in the presence of different mean wind shears, and (iv) the interaction of two solitons mediated by the presence of a mean wind shear.

Keywords Coupled KdV equations, Equatorial Rossby waves, Solitary waves, Atmospheric teleconnections
2000 MR Subject Classification 35Q51, 35Q53, 76B60, 86A10

1 Introduction

Energy exchange in the troposphere between the equatorial region and midlatitudes is a topic of considerable interest for understanding global teleconnection patterns from the tropics to midlatitudes, as well as the midlatitude influence on such tropical wave dynamics as monsoons. The possibility that the Madden-Julian or tropical intraseasonal oscillation is excited by midlatitude waves and can also drive midlatitude waves through its evolution and after its breakup has important consequences for weather predictability in the midlatitudes. The exchange of energy between equatorially trapped baroclinic waves and barotropic waves with a significant projection on the midlatitudes is, both, an important theoretical and applied issue.

Webster [26, 27] and Kasahara and Silva Dias [10] showed that localized, steady forcing of baroclinic waves in the tropics can drive a large, rapid response in barotropic waves with a

Manuscript received June 5, 2009. Published online August 18, 2009.
*Department of Mathematics, University of California at Davis, Davis, California 95616, USA.
E-mail: jabiello@ucdavis.edu
**Project supported by the National Science Foundation (No. DMS-0604947).

significant projection at midlatitudes when the zonal averaged winds have both vertical and meridional (latitudinal) shears. Hoskins and Jin [8] similarly studied the transient response to localized tropical forcing and emphasized the importance of nearly dispersionless equatorial Rossby waves in generating midlatitude barotropic waves. Wang and Xie [25] performed a linear stability analysis for an equatorial β-plane two-layer model around basic zonal states with both meridional and vertical shear. Their results showed that at large scales, equatorial Rossby waves strongly coupled to barotropic waves in the midlatitudes as linearized characteristic modes of propagation provided that there is vertical shear in the zonal background state; furthermore, the dispersion relation of the long wavelength, equatorial Rossby waves at large scales is modified significantly by the presence of a mean vertical shear.

Regarding the forcing of the tropics by midlatitude waves, Lim and Chang [15, 16] suggested the importance of vertical mean shear for a significant response, while Hoskins and Yang [9] emphasized the role of nearly resonant forcing in several specific physical mechanisms. Recently, Lin et al [17] showed the significance of midlatitude dynamics in triggering tropical intraseasonal responses in a climate model with essentially two vertical modes of resolution; a barotropic mode and a baroclinic heating mode.

These results inspired Majda and Biello [1, 2, 19] to develop a nonlinear theory describing the interaction of equatorial Rossby waves and barotropic waves with a significant midlatitude projection from a model where nonlinear advection is the only nonlinearity. Beginning with a two layer equatorial β-plane model as in [25–27], Majda and Biello [19] derived asymptotic equations governing the interaction of long equatorial baroclinic and barotropic waves in the presence of zonal mean shears; the long wave scaled equatorial Baroclinic-Barotropic equations. These equations describe nearly dispersionless long waves which are able to interact and exchange energy. Exploiting the fact that some of the Rossby waves can resonantly interact, the authors [19] developed a small amplitude theory of nearly dispersionless, long equatorial Rossby waves

$$\begin{aligned} 0 &= A_T - (1-2\gamma)A_{xxx} + (AB)_x, \\ 0 &= B_T - B_{xxx} + \Big(\frac{A^2}{2}\Big)_x, \end{aligned} \tag{1.1}$$

where A is the amplitude of an equatorially confined (baroclinic) Rossby wave packet and B is the amplitude of a (barotropic) Rossby wave packet with significant energy in the midlatitudes. The equations in (1.1) are written in the frame of reference moving with the Rossby waves and describe the modulation of the wave packet due to dispersion and nonlinearity on timescales of order 10 days. The parameter describing the difference in dispersion coefficients of the two waves, γ, varies depending on the north/south extent of the wave considered, but it is always positive, smaller than 0.06, and goes to zero for waves with large north/south wavenumber. It was shown in [19] that while equations (1.1) are derived through a weakly nonlinear theory, conservative values of the amplitude expansion parameter ($\epsilon \sim 0.1$, where ϵ is the Froude number) yield atmospherically relevant wind velocities and wave speeds. The x (longitudinal) means of these waves describe horizontal (in the case of B) and vertical and horizontal (in the case of A) wind shears. These mean values are clearly conserved by equations (1.1) and thus constitute parameters which describe the mean vertical and north/south shear in which the waves propagate: atmospheric scientists call this the climatology.

Using these equations, Majda and Biello [19] demonstrated that energy exchange between equatorial and midlatitude Rossby waves is greatly aided by the presence of vertical shear and occurs within 12 days for climatologically appropriate mean winds and shears.

Though these waves are coupled through vertical and north/south wind shear (the mean fields), the most intriguing aspect of the interaction is their nonlinear wave coupling. Under different physical assumptions, in the context of midlatitude baroclinic instability, Mitsudera [23] and Gottwald and Grimshaw [7] derived models using a weak β effect and resonant interaction which yielded pairs of KdV equations with nonlinear self interaction but only linear coupling, in contrast to the nonlinear cross wave coupling in [1, 2, 19] and equations (1.1).

In [2], Biello and Majda demonstrated a Hamiltonian structure for the amplitude equations (1.1) with a Hamiltonian which is cubic in the amplitudes. Furthermore, they constructed analytic solitary wave solutions with the functional form of the KdV soliton. These intriguing properties suggest that equation (1.1) has a rich structure which merits further study. In fact, a linear transformation recasts equation (1.1) in the form

$$\begin{aligned} U_T - (1-\gamma)U_{xxx} + UU_x &= \gamma V_{xxx} + \left(\frac{UV}{2}\right)_x, \\ V_T - (1-\gamma)V_{xxx} + VV_x &= \gamma U_{xxx} + \left(\frac{UV}{2}\right)_x, \end{aligned} \tag{1.2}$$

where, recall, γ is small. Notice, for $\gamma = 0$, $U = 0$ or $V = 0$ are invariant subspaces of the equations in (1.2) with the non-zero function evolving according to the KdV equation. This clearly shows that the nonlinear coupling of the waves is neither reducible nor negligible and, to this author's knowledge, neither equations (1.1) nor the equivalent (1.2) have appeared previously in the literature.

This paper has three goals. The first is to outline the derivation of equations (1.1) and (1.2) from a different perspective than [19], i.e. for readers interested in nonlinear wave equations, but not necessarily acquainted with the atmospheric science literature. In Section 2, the equatorial primitive equations are presented along with their non-dimensionalized scales, and their linear theory is discussed in Subsection 2.1. The long wave scaling and weakly nonlinear scalings are outlined separately in Subsection 2.2 and the important aspects of the derivation are presented in Subsection 2.3. The second goal is to give a physical interpretation of the structures, particularly the solitary waves, that are described by these equations. The transformation giving rise to the equations in (1.2) was not previously known and was discovered because of one simple property of (1.1). This transformation is presented in Section 3 where an atmospheric interpretation of the U and V solitons is also provided. The final goal is to gain an understanding of the interaction of these structures by examining solutions to equations (1.2). Though some solutions were presented in [19, 2], the novel structure of equations (1.2) allows their study from an entirely different perspective. In Subsection 3.1, the results of numerical integration of initial data consisting of one U and one V solitary wave are shown. Finally, Subsection 3.2 presents numerical solutions corresponding to one solitary wave in the presence of different vertical/latitudinal shears of longitudinal wind; such conditions more closely resemble the actual tropical atmosphere, where weak wind shears are known to effect the interaction of large scale waves.

2 The Equatorial Primitive Equations

The derivation begins with the unforced, incompressible, hydrostatic Euler equations on an equatorial β-plane

$$\begin{aligned} &\frac{\mathrm{D}}{\mathrm{D}t}u - \beta y v = -p_x, \\ &\frac{\mathrm{D}}{\mathrm{D}t}v + \beta y u = -p_y, \\ &\frac{\mathrm{D}}{\mathrm{D}t}\theta + N^2 w = 0, \\ &p_z = \theta, \\ &u_x + v_y + w_z = 0, \end{aligned} \tag{2.1}$$

where

$$\frac{\mathrm{D}}{\mathrm{D}t} = \frac{\partial}{\partial t} + u\frac{\partial}{\partial x} + v\frac{\partial}{\partial y} + w\frac{\partial}{\partial z} \equiv \frac{\partial}{\partial t} + (\vec{u}\cdot\nabla) \tag{2.2}$$

is the three-dimensional advective derivative, u, v and w are the longitudinal, latitudinal and vertical components of velocity, p is the pressure, and θ is the deviation of the potential temperature from a constant vertical gradient. The equator corresponds to $y = 0$.

The anelastic version of these equations are widely used in the atmospheric sciences to describe large scale (one thousand kilometers or larger) phenomena in the tropics (see, for example, [6, 18, 21, 24]). They form the basis of two theories developed by Majda and Biello: the nonlinear wave interaction theory (see [1, 2, 19]), on which this paper elaborates and the multi-scale theory of the Madden-Julian oscillation (see [3–5, 20]) which arises from an asymptotic analysis of (2.1) performed by Majda and Klein [21].

The troposphere is naturally periodic in the longitudinal (x) direction. On the other hand, in the y-direction, most of the waves described by equations (2.1) decay as Gaussians. These equatorially confined waves effectively behave as though they are in a channel with nearly no-penetration boundary conditions at latitudes suitably distant from the equator. There are a class of waves (barotropic Rossby waves) which do not decay with latitude, and the solution of these waves requires imposing the no-penetration boundary condition at midlatitudes (see [1]). In the vertical direction, the atmosphere is unbounded and the density of air decreases as different functions of height depending on the temperature stratification in the different layers. In this paper, I am only concerned with the weather layer, called the troposphere, which rises from the Earth's surface to a height of about 16 km in the tropics. The temperature stratification changes rapidly above this layer to the stratosphere immediately above it. Observations show that smaller scale waves do propagate from the troposphere to the stratosphere, but the stratification difference between these two layers acts like a sharp boundary between two fluids of different densities: much of the large scale wave activity which is forced in the troposphere remains confined to the troposphere. Thus, on the large scales, a rigid lid approximation at both the upper and lower boundaries has frequently been used as a simplifying approximation for these equations (see [6, 23, 25]) with observations supporting its use (see [13]).

The height of the troposphere, $H_T \approx 16$ km, and the rigid lid approximation, together, set a vertical length scale, $H = \frac{H_T}{\pi} \approx 5$ km. This scale, along with the Brunt-Väisälä frequency $N = 10^{-2}$ s^{-1}, defines the gravity wave speed $c = 50$ ms^{-1}. The remaining parameter in equation (2.1) is the latitudinal gradient of the Coriolis parameter evaluated at the equator, $\beta = 2.3 \times 10^{-11}$ ms^{-1}.

The first step in the analysis is to non-dimensionalize the variables in (2.1). The vertical length scale is measured in units of H, but this theory deals with horizontal length scales which are much longer, the so-called synoptic scale $L_E = (\frac{c}{\beta})^{\frac{1}{2}} = 1500$ km; these are the scales where the Coriolis force plays a significant role in the dynamics (see [21]). The natural time scale for wave propagation across this scale is the equatorial deformation time scale, $T_E = (c\beta)^{-\frac{1}{2}} \approx 8.3$ hrs $\approx \frac{1}{3}$ day. Therefore, the unit of horizontal velocity (u or v) is $\frac{L_E}{T_E} = c$, the gravity wave speed. In order for the vertical component of velocity to contribute to the divergence-free condition on the total velocity, the ratio of vertical to horizontal velocities must equal that of vertical to horizontal length scales. Therefore w is non-dimensionalized to $\frac{H}{T_E} = (\frac{H}{L_E})c \approx 16$ cms^{-1}. Furthermore, writing the primitive equations in the form (2.1) hides the fact that a temperature scale has already been chosen for θ — it is measured in units of the thermal lapse rate across one unit of the vertical scale, $\theta_0 \equiv 6.5$ K $\cdot$ km$^{-1} \times 5$ km ≈ 33 K.

Regarding the physical applicability of the asymptotics, horizontal velocities of 50 ms^{-1} when resolved over scales of 1500 km are absolutely too large and never observed in the tropical troposphere. Velocities of 5–10 ms^{-1} averaged over these length scales are consistent with the observational record (see [13]). Therefore, the weakly nonlinear asymptotics discussed below is motivated by, and relevant to the actual tropical atmosphere.

Henceforth, I shall work with the non-dimensionalized version of the equations in (2.1), which are attained by simply letting $N = \beta = 1$ in (2.1) and interpreting all of the variables as their non-dimensionalized counterparts.

2.1 Linear theory

The details of the linear theory of equatorial waves can be found in [18, Chapter 9] and were first derived by Matsuno [24] and re-derived by Gill [6], the most commonly cited reference. I will simply give an overview of the theory, highlighting the features which are important for the asymptotics.

Constructing the linearized version of equations (2.1) amounts to replacing the advective derivative with the partial time derivative. The no-penetration vertical boundary conditions implies $w = 0$ at $z = 0, \pi$. Therefore, the linear operator defined by (2.1) is skew self-adjoint using a norm of integration over $(x, y, x, t) \in \mathbb{R}^2 \times [0, \pi) \times \mathbb{R}$. The system is of constant coefficients in the vertical direction and an appropriate separation of variables ansatz which respects the vertical boundary conditions is $u, v, p \propto \cos(nz)$ and $w, \theta \propto \sin(nz)$,

$$\begin{bmatrix} u \\ v \\ w \\ p \\ \theta \end{bmatrix} = \begin{bmatrix} \widehat{u}_0(y) \\ \widehat{v}_0(y) \\ 0 \\ \widehat{p}_0(y) \\ 0 \end{bmatrix} \mathrm{e}^{\mathrm{i}(kx-\omega t)} + \sqrt{2} \sum_{n=1}^{\infty} \begin{bmatrix} \widehat{u}_n(y)\cos(nz) \\ \widehat{v}_n(y)\cos(nz) \\ \widehat{w}_n(y)\sin(nz) \\ \widehat{p}_n(y)\cos(nz) \\ \widehat{\theta}_n(y)\sin(nz) \end{bmatrix} \mathrm{e}^{\mathrm{i}(kx-\omega t)}, \tag{2.3}$$

and the different vertical modes decouple in the linear theory. The mode with subscript "0", which corresponds to horizontal winds which are independent of height, is called the equatorial barotropic mode.

Each element of the sum is called an equatorial baroclinic mode. These modes describe horizontal winds which are sheared with height. Furthermore, these are the modes which respond to heating, the primary driving mechanism for tropical dynamics. For example, forcing the $n = 1$ baroclinic mode corresponds to a $\sin(\pi z)$ forcing on the right-hand side of the

temperature equation in (2.1). This is the mode used to model the release of latent heat of condensation in the formation deep moist convection (such as systems of thunderstorms) in many theoretical studies (see [3, 11, 12, 20]).

The linear theory for the barotropic mode is most easily described since the lack of vertical velocity implies incompressibility in the horizontal direction. Upon introducing a stream function $\psi(x, y, t)$ for the velocity field, $u = -\psi_y$, $v = \psi_x$ and eliminating the pressure, it is straightforward to show that the equation governing the stream function is also constant coefficients in the y-direction. The solution of this equation is given by

$$\psi(x, y, t) \propto \mathrm{e}^{\mathrm{i}(kx+ly-\omega t)}$$

with dispersion relation

$$\omega_{bt} = -\frac{k}{k^2 + l^2}.$$

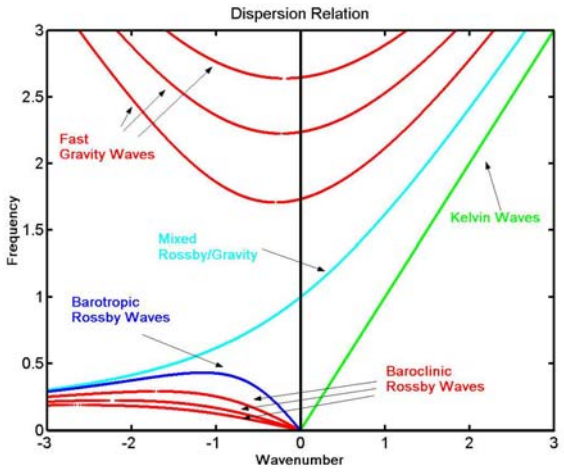

Figure 1 The non-dimensional dispersion relation of the barotropic Rossby wave and all of the waves of the first baroclinic mode. The y-wavenumber of the barotropic wave is arbitrarily chosen so that its dispersion curve would be distinguishable on this graph. Linear theory of long length- and time-scale asymptotics amounts to Taylor expanding the dispersion relation near the origin.

This curve is plotted in Figure 1 and is labeled the Barotropic Rossby wave. This wave is dispersionless in the long wave limit and its phase (and group) velocity approaches

$$c_{bt} = -\frac{1}{l^2}, \quad \text{as } k \to 0, \tag{2.4}$$

thus it travels westward along the equator. Notice that the energy density of this wave does not decay at higher latitudes and, in fact, it has infinite latitudinal extent. This should cause the reader to question whether or not the barotropic mode is actually the equatorial limit of some actual mode of the sphere. Previous work by Wang and Xie [25] has shown that the equatorial β-plane approximation is consistent with the longitudinally long modes of the sphere even for barotropic structures which are of large latitudinal extent. The unboundedness of this mode is

resolved by specifying no-penetration boundary conditions at fixed latitudes far enough away from the equator.

The latitudinal structure of the waves of the first baroclinic mode is determined by solving a second order ODE in y with eigenvalue ω_{bc}. The ODE is equivalent to Schroedinger's equation for a simple harmonic oscillator potential and the solutions are linear combinations of the parabolic cylinder functions (see [18]). The dispersion curves for the plethora of baroclinic waves is also shown in Figure 1. That they arise in several individual branches is a consequence of the fact that the quantum simple harmonic oscillator has only discrete spectrum. Each branch is described below.

There are an infinite number of fast inertio-gravity wave branches, only three of which are shown in Figure 1. The long wave limit of these waves is strongly dispersive and it is a regime which is not observationally relevant. (Note that shorter wavelength inertio-gravity waves make up a significant portion of the observed wave spectrum. For the definitive reference on observed waves in the equatorial troposphere, see Wheeler and Kiladis [28].) The branch of mixed Rossby/gravity waves in Figure 1 also has the property of being strongly dispersive at long longitudinal wavelengths. This wave is anti-symmetric about the equator and, while observations suggest that there is significant power in this mode (see [28]), the asymptotic limit considered in this paper does not capture such strongly dispersive behavior. The Kelvin wave is non-dispersive (at all wavelengths) and has the property that it travels eastward at the dry gravity wave speed (= 1 in non-dimensionalized units). This interesting wave has no latitudinal component in its velocity field and has a Gaussian profile about the equator. Its asymptotic behavior was studied by Majda et al [22].

The waves relevant to this paper are the equatorial baroclinic Rossby waves, three of whose branches are shown emanating from the origin in Figure 1. Like the barotropic Rossby waves these, too, are non-dispersive in the long wavelength limit. Unlike the barotropic waves, where l is a continuous variable, the discrete nature of the spectrum means that there are a countably infinite number of baroclinic Rossby wave branches. The baroclinic Rossby wave speed approaches

$$c_{bc} = -\frac{1}{2m+1} \quad \text{for } m = 1, 2, 3, \cdots, \quad \text{as } k \to 0, \tag{2.5}$$

where m is the index of the appropriate parabolic cylinder function (see [18]).

Like the barotropic Rossby wave, the baroclinic Rossby wave also travels westward along the equator, so there is the possibility that an equatorial baroclinic Rossby wave can resonantly exchange energy with an equatorial barotropic Rossby wave if

$$c_{bt} = c_{bc}. \tag{2.6}$$

For a given m baroclinic wave, the latitudinal wavenumber of the resonant barotropic wave is

$$l = \sqrt{2m+1} \quad \text{for } m = 1, 2, 3 \cdots. \tag{2.7}$$

The $m = 1$ Rossby wave is significant in the observational record (see [13]) and is an important component of the multi-scale MJO models (see [3, 20]). Its resonant barotropic counterpart has $l = \sqrt{3}$. The velocity vectors in the x, y-plane for both waves are shown in Figure 2. Since the barotropic wave is constant with height, the left panel of Figure 2 can be thought to correspond to either the bottom or top of the troposphere. The $n = 1$ baroclinic component in the right panel has the opposite sign at the bottom and top of the troposphere.

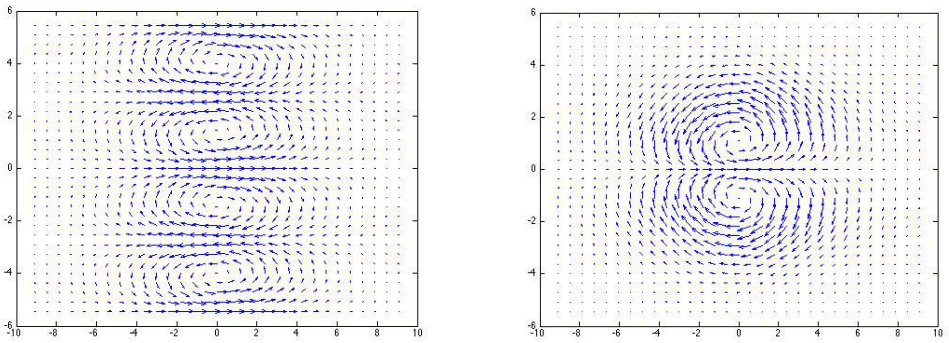

Figure 2 The left panel shows the horizontal velocity vectors in the (x, y)-plane of a barotropic Rossby wave packet with $l = 3$. The right panel shows the horizontal velocity vectors of the first baroclinic Rossby mode with $m = 1$. The horizontal velocity of this wave is of opposite sign at the top and bottom of the troposphere. The latitudinal extent of the panels is 6000 km north and south of the equator while the longitudinal extent is arbitrary. It is clear that the barotropic wave is significant at midlatitudes and the baroclinic wave is equatorially confined.

The structure of the linear eigenfunctions in the long wave limit merits mention because it determines the relative scaling of the fields in the asymptotics to follow. In the long wave limit, a scaling is chosen for the x derivatives, which are smaller than y or z derivatives. Consider the stream function formulation of the barotropic Rossby wave where v is proportional to the x derivative of the stream function while u is proportional to the y derivative. To maintain consistency with the linear theory, the ratio of v to u must be the same, at least formally, as the small ratio of x to y derivatives. Though it is not as obvious, the baroclinic Rossby waves also have this structure in the long wave limit. Furthermore, for long baroclinic waves, w scales as v; this can be seen by requiring all three terms to contribute to the incompressibility constraint in the long wave limit.

2.2 Long wave and small amplitude re-scaling

Consider the following rescaling of the variables in equations (2.1) in the limit of longitudinally long waves. In rewriting the equations, I will replace the variables with their rescaled counterparts. Let $\delta < 1$ be a small, positive parameter which defines a rescaling of the x variable so that partial derivatives are replaced by

$$\frac{\partial}{\partial x} \to \delta \frac{\partial}{\partial x}, \tag{2.8}$$

and the new scale for x is $\frac{L_E}{\delta}$. Non-dispersive long waves have the property that their frequency scales linearly with the wavenumber, which implies that the time derivative should be rescaled like the x derivative

$$\frac{\partial}{\partial t} \to \delta \frac{\partial}{\partial t}, \tag{2.9}$$

and the new scale for t is $\frac{T_E}{\delta}$. As was mentioned in the previous section, u is independent of wavenumber in the long wave limit, but v and w scale as the x derivative

$$u \to u, \quad v \to \delta v, \quad w \to \delta w, \tag{2.10}$$

so that the new velocity scale for v is δc and for w is $\delta(\frac{H}{L_E})c$. It is clear from the hydrostatic constraint that p and θ should scale in the same manner in the long wave limit, but it is less clear that they are both independent of k in this limit,

$$p \to p, \quad \theta \to \theta. \tag{2.11}$$

The physical reason for this balance is that any longitudinal flow in a rotating frame drives a latitudinal Coriolis force. In order to maintain small latitudinal velocities (in the long wave limit), the latitudinal pressure gradient must nearly cancel this force. Therefore the pressure must scale the same as the longitudinal velocity. Mathematically, this scaling is most easily seen from the linearized equation for the potential temperature. There are only two terms in this equation and both must scale in the same way in the limit that $\delta \to 0$, else both terms will be zero. Since w and the time derivative have already been scaled as $O(\delta)$, scaling $\theta \sim O(1)$ is the only way to achieve the balance.

Replacing all the variables in (2.1) with their rescaled counterparts and canceling factors of δ in the u equation and incompressibility constraint leads to the long equatorial wave equations

$$\begin{aligned}
&\frac{\mathrm{D}}{\mathrm{D}t}u - yv + p_x = 0,\\
&yu + p_y = -\delta^2 \frac{\mathrm{D}}{\mathrm{D}t}v,\\
&\frac{\mathrm{D}}{\mathrm{D}t}\theta + w = 0,\\
&p_z = \theta,\\
&u_x + v_y + w_z = 0,
\end{aligned} \tag{2.12}$$

where the advective time derivative is defined as in (2.2) with the rescaled variables (see [2, 19]). For $\delta = 0$, the linear theory of equations (2.12) describes all of the non-dispersive long wavelength modes seen in Figure 1 (the Kelvin waves and all types of Rossby waves), but it filters all of the fast waves (inertio-gravity and mixed Rossby/gravity). In particular, the equation for the v velocity becomes a constraint on the pressure in terms of the u velocity. This is called meridional geostrophic balance, and is unique to tropical waves.

The observational record indicates that large scale winds of 5–10 ms^{-1} are appropriate in the tropics; this is a factor of 5–10 less than the u velocity scale in equations (2.12). Define another small parameter

$$\epsilon \approx 0.1 \tag{2.13}$$

and replace all of the fields by their ϵ-rescaled counterparts

$$(u, v, w, p, \theta) \to \epsilon(u, v, w, p, \theta), \tag{2.14}$$

so that the unit for longitudinal velocities is now $\epsilon c = 5$ ms^{-1}. Substituting these rescalings into the equations in (2.12) and canceling one power of ϵ from each equation yields the weakly nonlinear long equatorial wave equations

$$\begin{aligned}
&u_t - yv + p_x = -\epsilon(\vec{u}\cdot\nabla)u,\\
&yu + p_y = -\delta^2 v_t - \delta^2\epsilon(\vec{u}\cdot\nabla)v,\\
&\theta_t + w = -\epsilon(\vec{u}\cdot\nabla)\theta,\\
&p_z = \theta,\\
&u_x + v_y + w_z = 0.
\end{aligned} \tag{2.15}$$

2.3 Amplitude equations for coupled Rossby waves

As in the derivation of the KdV equation, the nonlinear amplitude equation arises as a distinguished limit balancing dispersion and nonlinearity. Dispersion arises from the linear term in equation (2.15) that multiplies δ^2. Nonlinear interaction is due to the advection terms which multiply ϵ. Clearly, these two effects balance in the distinguished limit

$$\epsilon = \delta^2 \;\Rightarrow\; \delta \approx 0.3, \tag{2.16}$$

where the value of ϵ from equation (2.13) has been used. From this point forward, I shall use δ defined by the distinguished limit in equation (2.16) so that time is now measured in units of $\frac{T_E}{\delta} \approx 1$ day and the longitudinal scales in units of $\frac{L_E}{\delta} \approx 5000$ km.

A solution of the equations in (2.15) for $\epsilon = 0$ corresponding to a single barotropic and a single first baroclinic Rossby wave packet is

$$\begin{bmatrix} u \\ v \\ w \\ p \\ \theta \end{bmatrix}_R = \begin{bmatrix} -B(x-c_{bt}t)\widehat{\psi}_y \\ B_x(x-c_{bt}t)\widehat{\psi} \\ 0 \\ B(x-c_{bt}t)\widehat{P} \\ 0 \end{bmatrix} + \sqrt{2}\begin{bmatrix} A(x-c_{bc}t)\widehat{u}\cos(z) \\ A_x(x-c_{bc}t)\widehat{v}\cos(z) \\ A_x(x-c_{bc}t)\widehat{w}\sin(z) \\ A(x-c_{bc}t)\widehat{p}\cos(z) \\ A(x-c_{bc}t)\widehat{\theta}\sin(z) \end{bmatrix}. \tag{2.17}$$

The wave speed c_{bt} is defined in equation (2.4) and c_{bc} is defined in equation (2.5). All of the hatted variables depend only on y.

$$\widehat{\psi}(y) = -\sin(ly) \tag{2.18}$$

is the longitudinal structure of barotropic Rossby wave streamfunction ($\widehat{P}$ is not needed for the asymptotics), and

$$\begin{aligned} &-c_{bc}\widehat{u} - y\widehat{v} + \widehat{p} = 0, \\ &y\widehat{u} + \widehat{p}_y = 0, \\ &-c_{bc}\widehat{\theta} + \widehat{w} = 0, \\ &-\widehat{p} = \widehat{\theta}, \\ &\widehat{u} + \widehat{v}_y + \widehat{w} = 0 \end{aligned} \tag{2.19}$$

defines the longitudinal structure of the baroclinic Rossby wave eigenfunction. Restricting initial data to a single m-baroclinic Rossby wave and a barotropic Rossby wave which travels at the same speed, $c_{bt} = c_{bc}$ implies that the latitudinal wavenumber of the barotropic wave is given by equation (2.7); e.g. for $m = 1$, $l = \sqrt{3}$, as depicted in Figure 2.

I will now seek an asymptotic solution to the weakly nonlinear equation (2.15) for $\epsilon \neq 0$, $\epsilon \ll 1$, with initial data consisting of the two Rossby waves in (2.17),

$$\begin{bmatrix} u \\ v \\ w \\ p \\ \theta \end{bmatrix} = \begin{bmatrix} u \\ v \\ w \\ p \\ \theta \end{bmatrix}_R + \epsilon \begin{bmatrix} u_1 \\ v_1 \\ w_1 \\ p_1 \\ \theta_1 \end{bmatrix} + O(\epsilon^2). \tag{2.20}$$

The resulting equations at $O(\epsilon^0)$ are simply the linear long wave equations operating on the function defining the Rossby wave packet (2.17). By construction, this function satisfies the linear long wave equations so the $O(\epsilon^1)$ equations are identically zero.

At $O(\epsilon^1)$, the left-hand side of equation (2.15) are the linear long wave equations, now acting on the subscript "1" variables in equation (2.20). The right-hand side consists of the terms on the right-hand side of equation (2.15) evaluated using the Rossby wave variable from equation (2.17). Since both Rossby waves are traveling at the same speed, the right-hand side of equation (2.15) at $O(\epsilon^1)$ is constant in the frame of reference moving at this speed. In general, these terms will resonantly force the same Rossby waves in the $O(\epsilon^1)$ variables in equation (2.20), i.e.

$$\begin{bmatrix} u_1 \\ v_1 \\ w_1 \\ p_1 \\ \theta_1 \end{bmatrix} \propto t. \tag{2.21}$$

Therefore, the asymptotic expansion in equation (2.20) will no longer be well ordered when $\epsilon t \sim O(1) \Rightarrow t \sim \epsilon^{-1}$, which is about 10 days for the suggested choice of ϵ.

The ordering of the asymptotic expansion in equation (2.20) can be maintained by using the multiple time scales asymptotic procedure, allowing the Rossby wave packets at $O(\epsilon^0)$ to be modulated over the ϵt (long) time-scale,

$$\begin{aligned} B(x - c_{bt}t) &\to B(x - c_{bt}t, \epsilon t), \\ A(x - c_{bc}t) &\to A(x - c_{bc}t, \epsilon t), \end{aligned} \tag{2.22}$$

which amounts to incorporating all of the resonant behavior in the lowest order terms. Defining the long (10 day) time scale

$$T = \epsilon t, \tag{2.23}$$

the equations in (2.15) now become the multiple time-scale, weakly nonlinear long equatorial wave equations

$$\begin{aligned} &u_t - yv + p_x = -\epsilon[u_T + (\vec{u} \cdot \nabla)u], \\ &yu + p_y = -\epsilon v_t + O(\epsilon^2), \\ &\theta_t + w = -\epsilon[\theta_T + (\vec{u} \cdot \nabla)\theta], \\ &p_z = \theta, \\ &u_x + v_y + w_z = 0, \end{aligned} \tag{2.24}$$

where, using the distinguished limit δ^2 has been replaced by ϵ, and terms of $O(\epsilon^2)$ have been neglected since the resonant behavior occurs at $O(\epsilon^1)$.

The resonance that arises in equation (2.24) at $O(\epsilon^1)$ can now be removed by requiring that the inhomogeneous terms on the right-hand side (which are functions of operators acting on the wave packets, A and B) be non-resonant. This is achieved by invoking the Fredholm alternative which requires that the projection of the right-hand side against the adjoint eigenfunctions of the resonant waves, be zero.

The long wave linear operator in equation (2.24) is skew self-adjoint, a property which is inherited from the original linear operator. Therefore, the eigenfunctions of its adjoint operator are equal to its eigenfunctions. There are two such resonant eigenfunctions, one corresponding to each of the Rossby waves. The projection generates a dispersive, nonlinear evolution equation for the amplitudes of each of the Rossby wave packets

$$\begin{aligned} &r_A A_\tau - D_A A_{xxx} + \alpha B A_x + \beta A B_x = 0, \\ &r_B B_\tau - D_B B_{xxx} + \gamma A A_x = 0, \end{aligned} \tag{2.25}$$

where the coefficients are determined by the linear eigenfunctions

$$\begin{aligned} r_A &= \int_{-\infty}^{\infty} (\widehat{u}^2 + \widehat{p}^2)\mathrm{d}y, \\ D_A &= \frac{1}{2m+1}\int_{-\infty}^{\infty} \widehat{v}^2\mathrm{d}y, \\ \alpha &= \int_{-\infty}^{\infty} \widehat{\psi}_y[(\widehat{u}\widehat{v})_y - (\widehat{u}^2 + \widehat{p}^2)]\mathrm{d}y, \\ \beta &= -\frac{1}{2}\int_{-\infty}^{\infty} \widehat{\psi}_y[3\widehat{u}^2 + \widehat{p}^2]\mathrm{d}y \end{aligned} \tag{2.26}$$

for the baroclinic wave, and

$$\begin{aligned} r_B &= \pi l, \\ D_B &= \frac{\pi}{l^3}, \\ \gamma &= -\int_{-\infty}^{\infty} \widehat{\psi}_y[(\widehat{u}\widehat{v})_y + 2\widehat{u}^2]\mathrm{d}y \end{aligned} \tag{2.27}$$

for the barotropic wave.

Some comments about the equations:

(a) While the integrals in equations (2.26) and (2.27) are taken over all of $\mathbb{R}^1$, r_B and D_B are calculated by integrating over $-\frac{2\pi}{l} \leq y < \frac{2\pi}{l}$, i.e. one full period north and south of the equator. Since the barotropic Rossby wave is solved with no penetration at the northern and southern boundaries, one should also solve the baroclinic equations with these boundary conditions. However, since the baroclinic eigenfunctions decay as Gaussians away from the equator, solving them with such boundary conditions only adds an exponentially small correction to the functions — and, thereby, to the coefficients in equations (2.26) and (2.27). For simplicity, I have chosen the eigenfunctions corresponding to the unbounded domain, and I have evaluated the coefficients as integrals over this domain. The error incurred is negligible (see [25]) and does not change the structure of the amplitude equations (see [19]).

(b) The A-B nonlinearity only arises in the A-equation since $\cos(z) \times$ constant projects only onto $\cos(z)$, the baroclinic mode, not onto the constant (barotropic mode). The A-A nonlinearity only arises in the B-equation since $\cos(z) \times \cos(z)$ projects onto a constant (barotropic mode) and $\cos(2z)$ (though this is irrelevant for the asymptotics), but it does not project onto $\cos(z)$. A B-B nonlinearity does not occur in the A-equation since the product of constants is orthogonal to $\cos(z)$.

On the other hand, a B-B term could occur in the B-equation because it is a product of constants as a function of height — but it does not occur in this equation for a subtle reason. The barotropic self-advection term arises as though it were a two dimensional incompressible fluid, $J[\psi, \psi_{yy}]$, where $J[\psi, \phi] = \psi_x\phi_y - \phi_x\psi_y$ is the Jacobian. Since $\psi_{yy} = -l^2\psi$, the barotropic self-advection term is identically zero, without projection.

(c) It is straightforward to verify that the nonlinear coefficients have the property $\alpha - 2\beta + \gamma = 0$. This implies that the total wave energy

$$E = \int [r_A A^2 + r_B B^2]\mathrm{d}x \tag{2.28}$$

is conserved.

(d) The longitudinal mean of the barotropic wave is conserved:

$$\overline{B} = \int B \, \mathrm{d}x = \text{constant}. \tag{2.29}$$

Furthermore, it is shown by direct calculation that $\alpha = \beta$ (which, with the property (c) above implies that they both equal γ) so that the longitudinal means of the baroclinic amplitude is also conserved:

$$\overline{A} = \int A \, \mathrm{d}x = \text{constant}. \tag{2.30}$$

I emphasize that α and β are only equal when the wavenumber, l, is chosen appropriate to the resonance condition (2.7). It is neither obvious from the equations defining the coefficients (2.26), nor is it a property of the baroclinic eigenfunctions, alone. This is a subtle and important fact, which I have yet to completely understand.

(e) Rescaling the variables in equation (2.25) yields the system of equations (1.1) with

$$\gamma = \frac{1}{2(2m+1)^2}. \tag{2.31}$$

(f) Biello and Majda [2] described the Hamiltonian structure of (1.1) where the bracket is

$$\{F, G\} = -\int \Big[\frac{\delta F}{\delta A}\frac{\partial}{\partial x}\frac{\delta G}{\delta A} + \frac{\delta F}{\delta B}\frac{\partial}{\partial x}\frac{\delta G}{\delta B}\Big]\mathrm{d}x, \tag{2.32}$$

the Hamiltonian is

$$H = \frac{1}{2}\int [(1-2\gamma)(A_x)^2 + (B_x)^2 + A^2 B]\mathrm{d}x, \tag{2.33}$$

and the dynamics are given by $A_T = \{A, H\}$ and $B_T = \{B, H\}$.

(g) Linear theory for different mean values of $\overline{A}$ and $\overline{B}$ was studied in [19]. In [2], it was shown that at least one analytic solitary wave solution (for different values of $\overline{A}$ and $\overline{B}$) exists for $\gamma \neq 0$, and it has a $\mathrm{sech}^2(x)$ profile for both A and B. For $\gamma = 0$, two families of KdV solitons exist when the means $\overline{A} = \overline{B} = 0$.

3 Nonlinearly Coupled KdV Equations

A consequence of the top/bottom of the troposphere symmetry of the Rossby waves is that for every solution $(A(x,T), B(x,T))$ of the amplitude equations (1.1), $(-A(x,T), B(x,T))$ is also a solution; this is obvious from (1.1). It is also clear that, for $\gamma = 0$, $A = \sqrt{2}\,B$ is an invariant subspace of solutions; by the top/bottom symmetry, so is $A = -\sqrt{2}\,B$. In fact, letting either $A = \pm\sqrt{2}\,B$, then both equations in (1.1) become the KdV equation $B_T - B_{xxx} + 2BB_x = 0$. This suggests defining new variables where the invariance is manifest,

$$U = \frac{\sqrt{2}\,B + A}{\sqrt{2}} \quad \text{and} \quad V = \frac{\sqrt{2}\,B - A}{\sqrt{2}}, \tag{3.1}$$

so that the new variables evolve according to the equations in (1.2). Now the symmetry $A \to -A$ is realized as a symmetry upon interchange of $U \leftrightarrow V$.

Restricting attention to $\gamma = 0$, the equations in (1.2) become

$$\begin{aligned} U_T - U_{xxx} + UU_x &= \Big(\frac{UV}{2}\Big)_x, \\ V_T - V_{xxx} + VV_x &= \Big(\frac{UV}{2}\Big)_x. \end{aligned} \tag{3.2}$$

These are nonlinearly coupled KdV equations where either $U(x,T) = 0$ or $V(x,T) = 0$ is an invariant subspace. A soliton solution of system (3.2) is given by either

$$U(x,T) = S(x - \sigma T), \quad V(x,T) = 0, \quad \text{or} \quad U(x,T) = 0, \quad V(x,T) = S(x - \sigma T), \tag{3.3}$$

where

$$S(x) = -\frac{12}{\lambda^2}\operatorname{sech}^2\Big(\frac{x}{\lambda}\Big), \quad \sigma = -\frac{4}{\lambda^2}. \tag{3.4}$$

Figure 3 plots the wind vectors in the (x,y)-plane associated with this soliton solution. For $U = S$ and $V = 0$, the left panel shows the wind at the top of the troposphere and the right panel shows the wind at the bottom of the troposphere. The situation is reversed for $U = 0$ and $V = S$, so that the left panel shows the wind at the bottom, and the right panel shows the wind at the top of the troposphere.

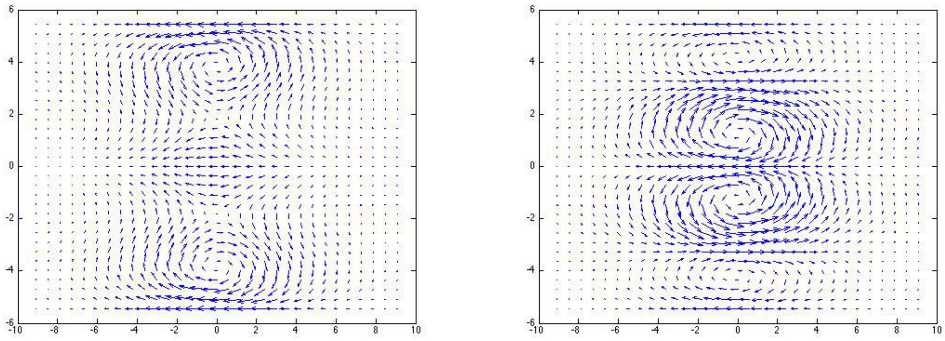

Figure 3 Velocity vectors in the (x,y)-plane associated with the soliton solution from equation (3.4). As in Figure 2, the latitudinal extent of the panels is 6000 km north and south of the equator while the longitudinal extent is arbitrary. For the soliton with $U = S$ and $V = 0$, the left panel shows the winds at the top of the troposphere, while the right panel shows the winds at the bottom of the troposphere. The plots are reversed for the soliton with $U = 0$ and $V = S$; the left panel shows the winds at the bottom of the troposphere, while the right panel shows the winds at the top of the troposphere.

Consider the U-soliton ($V = 0$), the structure of this flow is very interesting with regard to tropical/midlatitude connections. The soliton consists of a cyclonic flow at the top of the troposphere in the midlatitudes (the left panel). Furthermore, it consists of an anti-cyclonic pair of vortices at the bottom of the troposphere straddling the equator (the right panel). Conversely, the V-soliton ($U = 0$) consists of a cyclonic pair of vortices at the bottom of the troposphere in the midlatitudes (the left panel) coupled to an anti-cyclonic pair of vortices at the top of the troposphere straddling the equator (the right panel). Note that both solitons have easterly (i.e. coming from the east) winds at the equator at the bottom and top of the troposphere — though their strengths are significantly different. Also, for both solitons, the

winds are cyclonic in the midlatitudes, though their strength is different in the top and bottom of the troposphere.

Since this is an idealized model, many features of the real troposphere have been omitted; for example, coupling to active moisture is an important aspect of tropical wave dynamics (see [11, 28]). Nonetheless, these solitons suggest themselves as natural nonlinearly coupled tropical wave modes. The 10-day timescale is a reasonable one with regards to the observed lag time over which tropical activity can affect midlatitude weather forecasting. It is also a reasonable timescale over which waves from the midlatitudes are seen to excite organized tropical convection (see [14]); the solitons could be a natural conduit for such connections. Most intriguing, however, is that each soliton is an exact mode of the asymptotic equations which implies that the tropical/midlatitude interaction is, itself, described by these waves as a natural "mode" of the atmosphere. Exploring the relevance of these solitons to the observational record is an important future step in this work.

In the remaining sections of this paper, I will discuss the interaction of a U and a V soliton traveling at different velocities in Subsection 3.1, and I will study the effect of mean wind shears in the vertical and latitudinal direction on the behavior of a soliton in Subsection 3.2.

3.1 Interacting Rossby solitons without shear

Numerical integrations of the $\gamma = 0$ equations (3.2) are presented. A pseudo-spectral method was used to exactly solve the dispersion terms and fourth order Runge-Kutta time stepping was used to integrate the nonlinear terms. All solutions were monitored for conservation of energy, Hamiltonian and mean fields to a relative accuracy of at least 10^{-10}. A first test was performed to ensure that a single U soliton remained coherent — which it did for a thousand of time units, when the integration was stopped. A second test was performed to ensure that two U solitons would each remain coherent after collision — which they did for 20 collisions, when the integration was stopped.

In this subsection, I present numerical results showing the collision of one U-soliton with one V-soliton. For the U-soliton, $\lambda = 0.75$ and $\lambda = 1$ for the V-soliton (see equation (3.4)). Therefore the U-soliton is smaller amplitude, wider and slower than the V-soliton. The initial data is plotted in Figure 4(a), where the solid line is V and the dashed line is U. A word about notation is in order. I have chosen to use "soliton" to describe the solitary waves in either U or V when they are well separated and therefore evolve as solitons in the KdV system. After they interact, it is not clear that they remain solitons of the KdV system, and thus become "solitary waves".

The interaction is local, meaning that U and V essentially evolve according to uncoupled KdV equations until the solitons are close enough that the $(UV)_x$ term is significant. Detail of the interaction is shown in Figure 4(b). The smaller wave is changed dramatically during the interaction, splitting into two peaks, where the amplitude of the larger peak is a factor of 2 less than the original amplitude of the wave. Contrast this with two interacting solitons in the KdV equation where neither soliton amplitude decreases as dramatically. The trailing (right) end of the larger (V) wave increases to the point where it becomes positive. Since all soliton solutions of the uncoupled V equation must have negative amplitude, then this positive bump must project onto the radiation component of solutions to the KdV equation.

This radiation is clear in Figure 4(c), at a time well after the interaction has occurred.

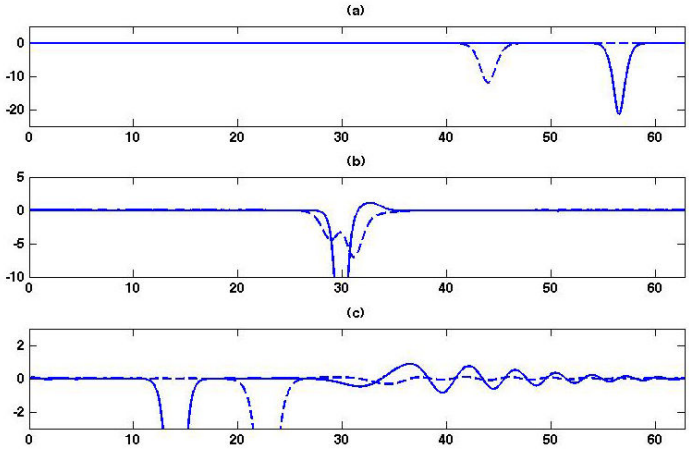

Figure 4 Snapshots of solitary wave heights at three different times. Solid curve is V, dashed curve is U. (a) Initial conditions showing two, well separated solitons. (b) Interaction detail at $T = 3.7$ showing the generation of positive V "radiation" to the right of the interaction. (c) Detail of radiation at $T = 5.95$.

The detail shows radiation in V traveling rightward and decaying to the right of the solitary waves. Its amplitude is everywhere $|V| < 1$; compare this to the initial height of the V soliton, $V_{\min} = -21.33$ at $T = 0$. Some radiation in U is also evident in this figure, though it is of much smaller amplitude than the V radiation. After the interaction the resulting height of the larger solitary waves is very slightly larger and the height of the smaller wave is very slightly smaller ($< 1\%$) than the respective heights of the original solitons.

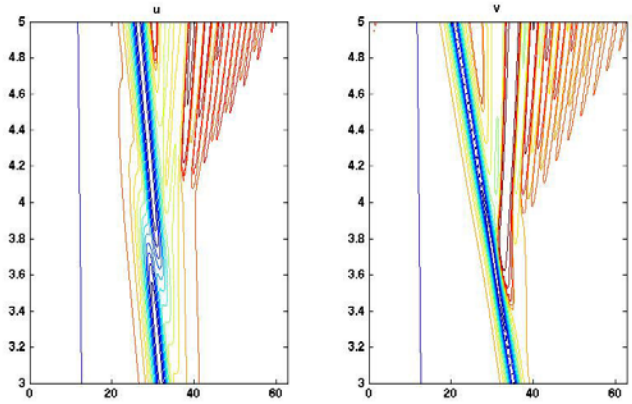

Figure 5 Contours of solitary wave height as a function of x and T near the interaction time. Left panel U, right panel V. Contour levels are different in each figure. The U solitary wave undergoes a phase shift during the interaction. Radiation to the right of the V solitary wave begins to form before the interaction maximum and travels to the right. Radiation in U seems to trail the radiation in V.

Figure 5 shows (x, T) contour plots of U (right panel) and V (left panel) around the time of the interaction. The minimum of the V wave is only slightly affected through the course of the interaction. However, at about $T = 3.4$, a significant peak of radiation is shed to the right

of this wave and it moves rightward with constant phase velocity. This peak is the first in a succession of smaller peaks, all of which are shed to the right of previous peaks. The front of this radiation moves rightward much faster than the constant phase velocity of the radiation. The radiation ceases to be generated at $T = 4.5$, when a distinct wedge appears between the solitary wave and its radiation field.

The U field (left panel of Figure 5) clearly shows the phase shift in the U solitary wave at $(x, T) = (30, 3.5)$. After the interaction, the solitary wave re-forms and appears to travel at the same speed as the original soliton, with the caveat that the amplitude is slightly smaller than before the interaction. The radiation in U parallels that in V; the front speed is faster than the phase speed, and the radiation eventually detaches from the solitary wave. Though the phase and front velocities appear to be the same for the U and V radiation, the U radiation significantly lags the V radiation and is not initiated until after the solitary wave interaction, when the waves begin to separate.

This radiation lag suggests that the U radiation may be formed in-situ from the V radiation. Because of the nature of the interaction term, the V radiation must contact some small, but non-zero U from which U radiation is generated. A candidate for this is the subtle "precursor" radiation which precedes the interaction and is visible in both the U and V fields. There is a contour in each of the U and V fields emanating from $T = 3$ at $x \approx 40$ and which moves very slowly to the left. Its velocity matches no other velocity in the figure — neither of the solitary waves nor their radiation phase or front speeds. This excess of U connects to the initial peak of U radiation at $(x, T) = (40, 4.1)$ and may act as a pre-conditioner from which V radiation can generate U radiation.

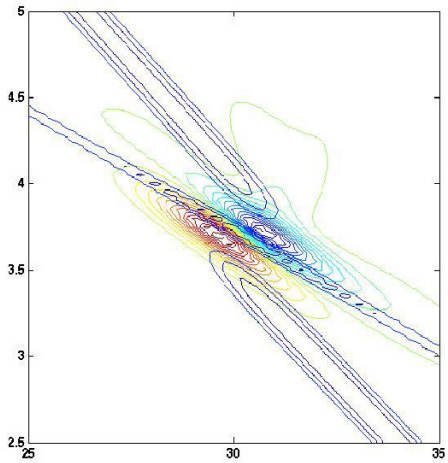

Figure 6 Detail of the solitary wave interaction as a function of x and T showing three contour levels for the V solitary wave (fast, unbroken) and the U solitary wave (slower, broken with phase shift). Also shown are contours of the interaction term, $(UV)_x$ which looks like a dipole in the contouring.

A final detailing of the solitary wave interaction is shown in the contour plot of Figure 6. Over-layed in this figure are a few of the extremal contours of the U and V solitary waves in addition to contours of the interaction term $(UV)_x$. The slower traveling U wave is clearly broken during the interaction and, at this resolution, seems to emanate unscathed. The V

wave decreases its amplitude (i.e. $V_{\min}$ increases) during the course of the interaction, but then appears to return to its original form. At the center of the collision, the interaction term appears as a dipole: sourcing U or V to the left of the interaction and sinking them to the right. This is consistent with the annihilation and re-creation of the U wave and the decrease and then increase in amplitude of the V wave. A more subtle feature of this figure is the long tail in the interaction term which precedes the interaction maximum, is slightly negative near the V wave and slightly positive near the U wave. This is a consequence of the exponential tails of the waves and should be important to further analyzing the interaction.

3.2 The effect of climatological wind shears

Clearly, the mean values of U and V are conserved by the dynamics in (3.2) and they correspond to values of mean vertical and longitudinal shear which are independent of time. In the first example with a mean shear, the initial data consists of a U solitary wave with $\lambda = 1$ and $V(x, 0) = 2.5$; contours of U and V are shown in Figure 7. The U solitary wave remains coherent for the whole integration time and there is only a small amount of rightward traveling radiation generated. The V solution consists of a component which is strongly tied to the U wave plus radiation traveling to the right. Both of these components are about the same strength, and both are much weaker than the U solitary wave.

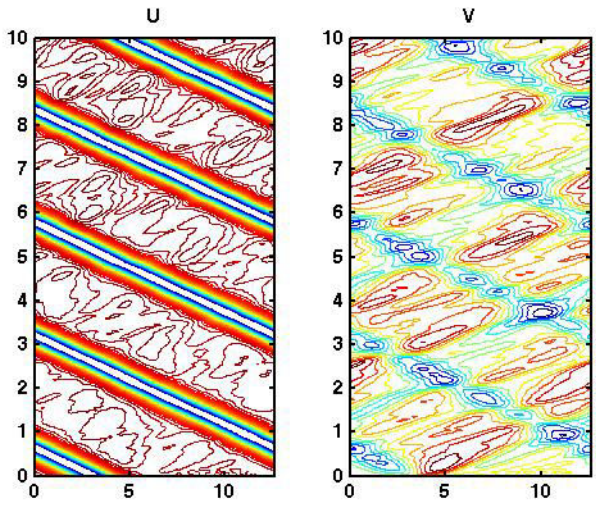

Figure 7 U (left panel) and V (right panel) as a function of x and T for initial conditions with U as a $\lambda = 1$ solitary wave and $V(x, 0) = 2.5$. The U wave travels at constant leftward velocity with a small amount of radiation to the right. The V solution consists of a component strongly coupled to U plus radiation to the right. The contour levels are the same for the two panels, so it is clear that V is of much smaller magnitude than U.

Contrast this with the example shown in Figure 8 which has the same U solitary wave initial condition, but with $V(x, 0) = -2.5$. Within two time units the interaction of the U solitary wave with the background flow causes a V solitary wave to be formed in its wake. The V wave actually travels faster than the U wave and they collide at $T = 4.5$. Much like the example of two solitary waves in Subsection 3.1, the slower, U wave is split and phase shifted by this

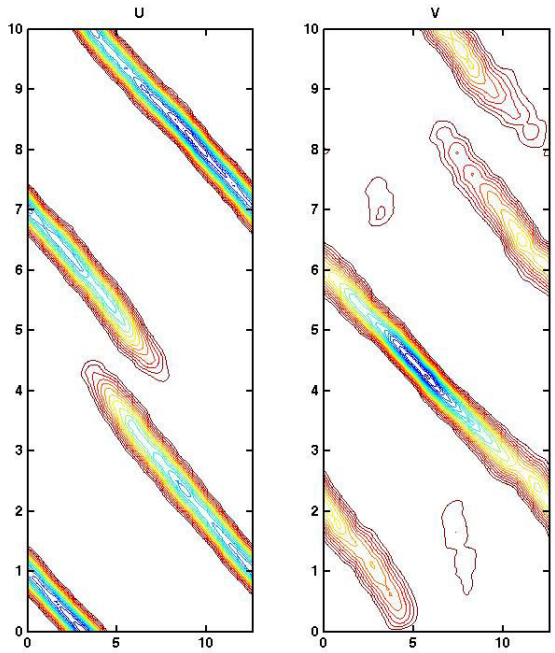

Figure 8 U (left panel) and V (right panel) as a function of x and T for initial conditions with U as a $\lambda = 1$ solitary wave and $V(x,0) = -2.5$. The U wave quickly generates a V wave in its wake. Their first interaction causes the U wave to split while their second interaction causes the V wave to split.

interaction. However, at $T = 8$ the waves interact again and this time the V solitary wave is split and phase shifted by U: a sort of hopscotch.

There is significant wave radiation generated by these interactions, which does not show up on the contouring, and which repeatedly interacts with the solitary waves. Figure 9 shows the U and V contours over a long period of time. After $T = 25$, the V wave settles into a coherent leftward traveling state with some rightward traveling radiation evident. The repeated interaction of the U solitary wave with the V solitary wave eventually causes the breakup of the U wave. Around $T = 80$ there is only a trace of the U wave remaining, though bursts of activity still travel leftward. For example, pairs of bursts can be seen at $(x,T) = (7,85)$, $(11,92)$ and $(6,96)$. These bursts occur on either side of the traveling V wave and most likely result from U radiation interacting with the V solitary wave.

The final example considers the effect of a background mean state on the interaction of the two solitary waves considered in Subsection 3.1. To the V initial condition is added a constant, $\overline{V} = 5$. It was already shown in the first example of this section that a U solitary wave interacting with a positive $\overline{V}$ background only generates some rightward traveling radiation. Additionally, the effect of $\overline{V}$ on the V-solitary wave is to embed it in a rightward blowing wind, i.e. to slow its leftward propagation. Contours in $U(x,T)$ and $V(x,T)$ are shown in Figure 10. Although the U wave is weaker, because of the mean $\overline{V}$ it travels faster than the V wave.

The first interaction occurs at $(x,T) = (8,1.5)$ although, as in the example in Subsection 3.1, there is significant rightward traveling radiation emanating from the U-wave prior to the interaction. The V wave is drastically altered, losing amplitude and velocity after the interac-

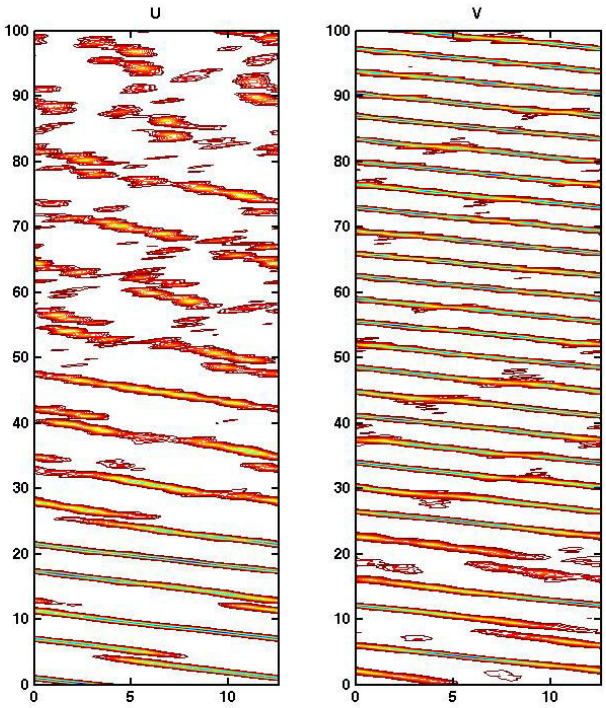

Figure 9 U (left panel) and V (right panel) as a function of x and T for initial conditions with U as a $\lambda = 1$ solitary wave and $V(x,0) = -2.5$, for a long integration time. After repeated interactions, a coherent V wave is formed and persists while the U wave ceases to be coherent. The extrema of the U wave avoid the extrema of the V wave after $T = 50$.

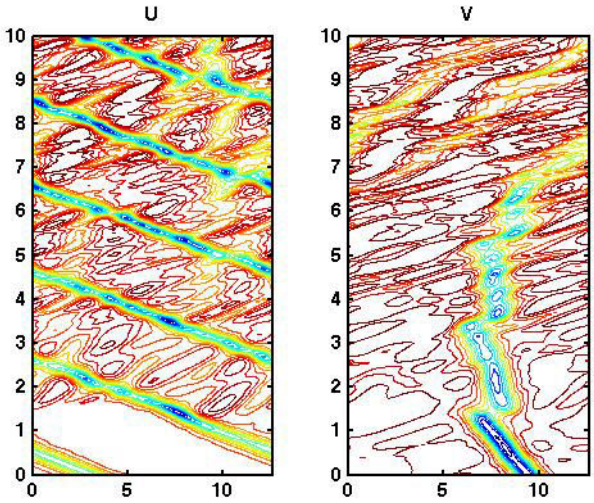

Figure 10 The two solitary waves of the example in Figure 5 plus a mean $\overline{V} = 5$. The wave interaction repeatedly slows and disturbs the V solitary wave until it splits in two right moving waves.

tion. During the interaction, the amplitude of the U wave increases, which is the opposite of what happens in the case with no mean field. It then begins to collide with the radiation field that it generated and seems likely to break up around $T = 2.5$, but survives.

In the second interaction, the U wave again increases in amplitude, but approximately returns to its original amplitude after the interaction is complete. Strong U radiation is released rightward of the point $(x, T) = (7, 3.5)$. The V wave again slows down and weakens, but less than in the first interaction. After $T = 3.5$, there is a distinct rightward traveling radiation component in V. The V-solitary wave repeatedly collides with this radiation and appears more like a blinking state than a coherent wave.

After the third interaction, the V wave becomes a stationary blinking mode. The fourth interaction occurs at $(x, T) = (10, 7)$ and there appear to be two slightly coherent V-solitary wave structures traveling rightward at speed 3. These could be weak solitary waves being advected by the background $\overline{V}$, but by $T = 10$, they appear to be completely absorbed by the faster, rightward traveling V radiation. The U solitary wave repeatedly interacts with its own radiation and, of course, the disorganized radiation and mean field of V. However, it returns to a coherent state after each interaction.

There is broad range of interesting and unexplained of behavior being displayed in just these few numerical examples. A detailed analysis of the soliton collision, radiation and interaction with shear is beyond the scope of this paper, but will be addressed in future work. Furthermore, much more work is necessary in order to understand the implications of these structures and interactions for atmospheric tropical/midlatitude connections.

Acknowledgements The author dedicates this work to Andy Majda on the occasion of his 60th birthday with thanks for teaching the author about the richness of the mathematics and physics of the atmospheric sciences. Thank J. K. Hunter for so many illuminating discussions about nonlinear waves.

References

[1] Biello, J. A. and Majda, A. J., Boundary layer dissipation and the nonlinear interaction of equatorial baroclinic and barotropic Rossby waves, *Geophys. Astrophys. Fluid Dyn.*, **98**(2), 2004, 85–127.

[2] Biello, J. A. and Majda, A. J., The effect of meridional and vertical shear on the interaction of equatorial baroclinic and barotropic Rossby waves, *Stud. Appl. Math.*, **112**(4), 2004, 341–390.

[3] Biello, J. A. and Majda, A. J., A new multiscale model for the Madden-Julian oscillation, *J. Atmos. Sci.*, **62**(6), 2005, 1694–1721.

[4] Biello, J. A. and Majda, A. J., Modulating synoptic scale convective activity and boundary layer dissipation in the IPESD models of the Madden-Julian oscillation, *Dyn. Atmos. Oceans*, **42**(1–4), 2006, 152–215.

[5] Biello, J. A. and Majda, A. J., Transformations for temperature flux in multiscale models of the tropics, *Theor. Comput. Fluid Dyn.*, **20**(5–6), 2006, 405–420.

[6] Gill, A. E., Some simple solutions for heat-induced tropical circulations, *Quart. J. Roy. Meteor. Soc.*, **106**(449), 1980, 447–462.

[7] Gottwald, G. and Grimshaw, R., The formation of coherent structures in the context of blocking, *J. Atmos. Sci.*, **56**(21), 1999, 3640–3662.

[8] Hoskins, B. J. and Jin, F.-F., The initial value problem for tropical perturbations to a baroclinic atmosphere, *Quart. J. Royal. Meteor. Soc.*, **117**(498), 1991, 299–317.

[9] Hoskins, B. J. and Yang, G.-Y., The equatorial response to higher-latitude forcing, *J. Atmos. Sci.*, **57**(9), 2000, 1197–1213.

[10] Kasahara, A. and Silva Dias, P. L. da, Response of planetary waves to stationary tropical heating in a global atmosphere with meridional and vertical shear, *J. Atmos. Sci.*, **43**(18), 1986, 1893–1912.

[11] Khouider, B. and Majda, A. J., A simple multicloud parameterization for convectively coupled tropical waves, Part I: linear analysis, *J. Atmos. Sci.*, **63**(4), 2006, 1308–1323.

[12] Khouider, B. and Majda, A. J., Multicloud convective parametrizations with crude vertical structure, *Theor. Comput. Fluid Dyn.*, **20**(5–6), 2006, 351–375.

[13] Kiladis, G. N. and Wheeler, M., Horizontal and vertical structure of observed tropospheric equatorial Rossby waves, *J. Geophys. Res.*, **100**(D11), 1995, 22981–22997.

[14] Kim, B.-M., Lim, G.-H. and Kim, K.-Y., A new look at the midlatitude-MJO teleconnection in the northern hemisphere winter, *Quart. J. Roy. Meteor. Soc.*, **132**(615), 2006, 485–503.

[15] Lim, H. and Chang, C.-P., A theory for midlatitude forcing of tropical motions during winter monsoons, *J. Atmos. Sci.*, **38**(11), 1981, 2377–2392.

[16] Lim, H. and Chang, C.-P., Generation of internal- and external-mode motions from internal heating: effects of vertical shear and damping, *J. Atmos. Sci.*, **43**(9), 1986, 948–960.

[17] Lin, J. W.-B., Neelin, J. D. and Zeng, N., Maintenance of tropical intraseasonal variability: impact of evaporation-wind feedback and midlatitude storms, *J. Atmos. Sci.*, **57**(17), 2000, 2793–2823.

[18] Majda, A. J., Introduction to PDEs and Waves for the Atmosphere and Ocean, AMS, Providence, RI, 2003.

[19] Majda, A. J. and Biello, J. A., The nonlinear interaction of barotropic and equatorial baroclinic Rossby waves, *J. Atmos. Sci.*, **60**(15), 2003, 1809–1821.

[20] Majda, A. J. and Biello, J. A., A multiscale model for tropical intraseasonal oscillations, *Proc. Natl. Acad. Sci.*, **101**(14), 2004, 4736–4741.

[21] Majda, A. J. and Klein, R., Systematic multiscale models for the tropics, *J. Atmos. Sci.*, **60**(2), 2003, 393–408.

[22] Majda, A. J., Rosales, R. R., Tabak, E. G., et al, Interaction of large-scale equatorial waves and dispersion of Kelvin waves through topographic resonances, *J. Atmos. Sci.*, **56**(24), 1999, 4118–4133.

[23] Mitsudera, H., Eady solitary waves: a theory of type B cyclogenesis, *J. Atmos. Sci.*, **51**(21), 1994, 3137–3154.

[24] Matsuno, T., Quasi-geostrophic motions in the equatorial area, *J. Meteor. Soc. Japan*, **44**(1), 1966, 25–43.

[25] Wang, B. and Xie, X. S., Low-frequency equatorial waves in vertically sheared zonal flow, Part 1: stable waves, *J. Atmos. Sci.*, **53**(3), 1996, 449–467.

[26] Webster, P. J., Response of tropical atmosphere to local, steady forcing, *Mon. Wea. Rev.*, **100**(7), 1972, 518–541.

[27] Webster, P. J., Mechanisms determining the atmospheric response to sea surface temperature anomalies, *J. Atmos. Sci.*, **38**(3), 1981, 554–571.

[28] Wheeler, M. and Kiladis, G. N., Convectively coupled equatorial waves: analysis of clouds and temperature in the wavenumber-frequency domain, *J. Atmos. Sci.*, **56**(3), 1999, 374–399.